Bioactive Materials 4 (2019) 132–141

Contents lists available at ScienceDirect

Bioactive Materials

journal homepage: http://www.keaipublishing.com/biomat

Surface bioactivation of PEEK by neutral atom beam technology

Joseph Khoury[a,*], Irina Selezneva[b], Sergei Pestov[c], Vadim Tarassov[d], Artem Ermakov[b], Andrey Mikheev[b], Mikhail Lazov[c], Sean R. Kirkpatrick[a], Dmitry Shashkov[a], Alexandre Smolkov[c]

[a] Exogenesis Corporation, Billerica, MA, USA
[b] Institute of Theoretical and Experimental Biophysics, Russian Academy of Sciences, Pushchino, Moscow Region, Russia
[c] MIREA – Russian Technological University, Moscow, Russia
[d] OAO Technotransservice Engineering, Moscow, Russia

A B S T R A C T

Polyetheretherketone (PEEK) is an alternative to metallic implants and a material of choice in many applications, including orthopedic, spinal, trauma, and dental. While titanium (Ti) and Ti-alloys are widely used in many intraosseous implants due to its biocompatibility and ability to osseointegrate, negatives include stiffness which contributes to shear stress, radio-opacity, and Ti-sensitivity. Many surgeons prefer to use PEEK due to its biocompatibility, similar elasticity to bone, and radiolucency, however, due to its inert properties, it fails to fully integrate with bone. Accelerated Neutral Atom Beam (ANAB) technology has been successfully employed to demonstrate enhanced bioactivity of PEEK both *in vitro* and *in vivo*. In this study, we further characterize surfaces of PEEK modified by ANAB as well as elucidate attachment and genetic effects of dental pulp stem cells (DPSC) exposed to these surfaces. ANAB modification resulted in decreased contact angle at 72.9 ± 4.5° as compared to 92.4 ± 8.5° for control ($p < 0.01$) and a decreased average surface roughness, however with a nano-textured surface profile. ANAB treatment also increased the ability of DPSC attachment and proliferation with considerable genetic differences showing earlier progression towards osteogenic differentiation. This surface modification is achieved without adding a coating or changing the chemical composition of the PEEK material. Taken together, we show that ANAB processing of PEEK surface enhances the bioactivity of implantable medical devices without an additive or a coating.

1. Introduction

Over the past two decades, polyetheretherketone (PEEK) has been increasingly used as an alternative to metal implants in orthopedic and dental surgery because of its mechanical and biological properties as well as its radiolucency. One of the main reasons to use PEEK in place of metal alloys is to eliminate concerns regarding potential metal allergies [1,2]. The ability to manipulate the modulus of elasticity of PEEK to more closely match that of bone reduces the possibility of stress shielding and bone resorption. Despite the benefits of PEEK, its inert nature means that it fails to promote an adequate bone integration. Many studies have investigated surface modification methods to augment direct bone-implant contact. These methods include physical treatments (plasma) [3], chitosan film deposition [4–6], chemical treatment [7], calcium phosphate or titanium surface coatings [8–11], as well as the use of composites with hydroxyapatite (HA) [12,13]. However, the clinical success of these treatments may be limited because of reduced strength of the PEEK substrate and delamination of various coatings in physiological environments due to the stress concentration at the PEEK-coating interface [14]. While titanium implants have been the standard in dental and many orthopedic applications, they are increasingly being recognized to elicit either an immediate (type I, antigen/antibody based) or delayed (type IV, cell-mediated) allergen response in a subset of individuals, which may cause implant failure in these patients [15].

In continuation of previous studies, we have employed a relatively recent technology called Accelerated Neutral Atom Beam (ANAB) that can modify the surface of an implantable medical device to a shallow depth of no greater than 2–3 nm [16,17]. The ANAB technique, described earlier in detail [18], employs an intense directed beam of neutral gas atoms, which have average energies that can be controlled over a range from a few electron volts (eV) to over 100 eV per atom. These neutral atom beams are produced by dissociating energetic gas cluster ions produced by the Gas Cluster Ion Beam (GCIB) technique [19].

The first goal of this study was to further characterize the effects of ANAB treatment on the surface chemistry and bioactivation of PEEK. Secondly, we aim to establish a fundamental understanding of the genetic mechanism behind stem cell interactions with ANAB-modified PEEK surface. We accomplish that by assaying the ability of dental pulp stem cells (DPSC) to maintain their stemness, enhance their proliferative ability and differentiate towards bone on the modified

Peer review under responsibility of KeAi Communications Co., Ltd.
* Corresponding author.
E-mail address: jkhoury@exogenesis.us (J. Khoury).

https://doi.org/10.1016/j.bioactmat.2019.02.001
Received 26 October 2018; Received in revised form 31 January 2019; Accepted 9 February 2019
Available online 21 February 2019

surface.

2. Materials and methods

2.1. Sample preparation

PEEK films (0.1 mm thick, Solvay Plastics) were cut to 5 mm × 5 mm coupons. PEEK coupons were then either left as control or further treated by ANAB processing on an nAccel100 accelerated beam processor (Exogenesis Corp, Billerica, MA) at an effective dose of 5×10^{16} argon (Ar) atoms per cm^2. PEEK coupons were sterilized prior to studies by autoclaving for 45 min at 121 °C and pressure P = 0.5 atm.

2.2. X-ray photoelectron spectroscopy (XPS)

The photoelectron spectra of the PEEK samples were obtained on an ESCALAB MKII electronic spectrometer (VG SCIENTIFIC, UK) equipped with a monochromatic Mg-K_α source at 1253.6 eV and operating at 50 W power. The micro-focused X-ray beam was raster scanned to an analysis area of 200 μm × 200 μm. The energy of the emitted electrons was measured with a hemispherical energy analyzer at pass energy of 20 eV with step change of 0.1–0.2 eV for high-resolution spectra and 50 eV with step change of 0.5 eV for survey spectra. The binding energy (BE) scale was referenced to the C-C peak maximum in the C 1s spectra at 284.8 eV. Dual beam charge neutralization eliminated any sample charging. Typical pressures in the analysis chamber during spectral acquisition were equivalent to 5×10^{-9} mbar (5×10^{-7} Pa). A qualitative analysis based on the known chemical formula of PEEK and possible impurities was performed, followed by a quantitative characterization of the atomic concentrations in a thin surface film.

The qualitative composition was performed according to the atlas of the XPS spectra [20–22] and the online databases [22,23]. In quantitative analysis, the following formula was used:

$$X_i = \frac{S_i/(\sigma_i \cdot \lambda_i)}{\sum_j S_j/(\sigma_j \cdot \lambda_j)}$$

Where, X_i is the atomic concentration, S_i is the area under the corresponding XPS peak, σ_i is the photoionization cross-section for the selected element line using the data from CASA XPS database [22], and λ_i is the mean free path of the characteristic electrons in the sample for each corresponding line. At detection angles close to normal, we used the Cumpson approximation for the ratio of electron mean free paths [24]:

$$(\lambda_1/\lambda_2) = (E_{kin\ 1} / E_{kin\ 2})^{0.75}$$

Then the formula is transformed into:

$$X_i = \frac{S_i/(\sigma_i \cdot [E_{h\nu} - E_{\text{св},i}]^{0.75})}{\sum_j S_j/(\sigma_j \cdot [E_{h\nu} - E_{\text{св},j}]^{0.75})}$$

Where $E_{kin\ 1,2}$ is the kinetic energy of the electron, $E_{h\nu}$ is the energy of the X-ray photon (1253.6 eV), $E_{bond,i}$ is the binding energy of the given line/peak. The calculations also used the mean free paths calculated by the QUASES-IMFP-TPP2M program [25] using the Tanum-Powell-Penn TPP-2M formula [26].

2.3. IR spectroscopy

The IR-Fourier spectrum of PEEK samples was recorded on a Bruker Equinox 55 instrument in the middle IR range without special sample preparation, with the aid of a mirror attachment from PIKE Technologies Inc., and the angle of incidence of 30°. The acquired spectrum was transformed to the form of absorption and processed using OPUS_6.0 software [27] and other published data from Refs. [28,29].

2.4. Atomic force microscopy

Measurement of the surface roughness of polymer films was carried out using a scanning probe atomic force microscope Smart SPMTM-1000 in a semi-contact mode at a resonant cantilever frequency of 260.6 kHz and an amplitude of 20 nm. The root-mean-square surface roughness was analyzed in the IAPro 2.0.10 program. The average surface roughness was determined from the data of three 10 μm × 10 μm scans for each of the samples.

2.5. Contact angle evaluation

Contact angle was measured using the sessile drop method on a manual simplified device. A 2 μl droplet of deionized water, physiologic saline solution, or fetal bovine serum (FBS) at room temperature (20 °C) was placed on the flat PEEK surfaces and imaged on a stand using a 5-megapixel PL-A741 (PixeLINK) video camera, an OBJ-11 MMS (Edmund Optics), and Fiber-Lite DC-950 (Dolan-Jenner Industries) system, providing uniform illumination. The droplet angles were measured by ImageJ software (NIH) with the Contact Angle plugin. Five individual evaluations for each condition were measured and averaged to compare treated and untreated PEEK surfaces. The statistical significance between the groups was calculated using the Mann–Whitney *U* test, values of $p < 0.05$ were considered significant.

2.6. Cell culture

Human tooth postnatal dental pulp stem cells (DPSC) were isolated from the rudiment of the third molar extracted by orthodontic indications as previously described [30]. Cells were grown in DMEM/F12 medium supplemented with 10% fetal calf serum (FBS, HyClone) in a humidified incubator, at 37 °C, and 5% CO_2. The medium was changed after 24 h in the primary cell culture, then 48 h later. The cells were maintained until formation of dense growth islets or formation of a monolayer of cells and then passaged for growth. Cells in the third and fourth passages were used for this study.

2.7. Transgenic cell cultures GFP-DPSC preparation

LVT-TagGFP2 lentivector (Eurogen, Russia) was used for producing the transgenic cultures of DPSC cells carrying the green fluorescent protein gene (GFP-DPSC). The cells were transduced according to Moffat J. et al. [31], briefly DPSC from the 2nd passage were maintained in a 24 well plate at 10^4 cells/well. A day after seeding, 10^5 lentiviral particles were added to the culture medium; the culture medium was changed after one day. On day 3 after infection, the development of GFP expression by fluorescence level was observed in the cells using a fluorescence microscope. 2 μg/ml Puromycin (Santa Cruz, USA) was added, and the antibiotic selection of the cells was carried out for 5 days. The resulting cell culture (GFP-DPSC) was used to study the adhesion and growth of cells on the surface of PEEK by fluorescence microscopy.

2.8. Determination of adhesive characteristics of material surfaces and their ability to maintain cell proliferation

GFP-DPSC cells were seeded on control or ANAB-treated PEEK (5 mm × 5 mm, n = 3 per study) at a concentration of 40,000 cells/cm^2 (DMEM/F12 + 10% FBS medium) in 24-well dishes, glass slides of the same size were used as controls. One (1) and 3 days after seeding, cells on the surface of the materials were imaged using an Axiovert 200 fluorescent microscope with, λ_{excit} = 450–490 nm, and λ_{emiss} = 515–565 nm. Samples were then prepared for Scanning Electron Microscopy (SEM). PEEK or glass slides with GFP-DPSC were washed in 0.1 M phosphate-buffered saline (pH 7.4) and fixed for 12 h at 5 °C in a 2.5% buffered solution of glutaraldehyde. After fixation, the

samples were washed with water and dehydrated at 4 °C in increasing concentrations of ethanol: 50%, 75%, 80%, 90%, and 100%; two rinses of 5 min in each concentration. Samples were then placed in hexamethyldisilazane (HMDS) for 30 min, and then air dried. The microstructure of the samples was studied using a scanning electron microscope with a Tescan Vega II field emission source (TESCAN, Czech Republic) in secondary electrons (a SE detector) at an accelerating voltage of 20 kV.

2.9. Cell attachment and proliferation

Cell attachment and proliferation were studied on PEEK coupons or glass slides using 24-well dishes at a concentration of 40,000 cells/cm^2 in DMEM/F12 + 10% FBS.

At each time point, cells were stained with SYTO 9 and propidium iodide and the viability of the cells was assessed using an Axiovert 200 fluorescent microscope at λ_{excit} = 450–490 nm, and λ_{emiss} = 515–565 nm for living (green) cells and at λ_{excit} = 546 nm, and λ_{emiss} = 575–640 nm for dead (red) cells.

2.10. Gene expression study

DPSC cells were seeded on control or ANAB-treated PEEK coupons or glass slides (5 mm × 5 mm, n = 4 for each study) at a concentration of 40,000 cells/cm^2 (DMEM/F12 + 10% FBS medium) in 24-well dishes for 1, 15, and 35 days. Media was changed every 3 days.

RNA from cells was prepared using the isolation of full-length poly (A) mRNA on magnetic particles (Sileks, Moscow). The resulting mRNA was used for the synthesis of complementary DNA (oligo (dT) 15, Sileks). cDNA was then used as a template for real-time PCR, which was performed on an ABI Prism 7500 Sequence Detection System (Applied Biosystems) instrument using a Synthol kit containing SybrGreen intercalating dye and a reference ROX dye. Marker genes were selected from the PCR profiling database from Qiagen (http://www.sabiosciences.com). The primers for each marker gene were selected using the PrimerEpress program (Applied Biosystems); the primer length averaged 24 nucleotides, and the length of the amplified fragment is 94–100 nucleotide pairs. The reaction was carried out according to the following scheme: 1 cycle 95 °C - 5 min; 2 - 40 cycles 95 °C - 30 s, 60 °C - 40 s; 1 cycle (dissociation stage) 95 °C - 15 s, 60 °C - 1 min, 95 °C - 15 s.

The amplification products were checked by electrophoresis in 2% agarose for verification of the specificity of the reaction. Real-time analysis of the data was performed by threshold fluorescence using the $2^{-\Delta\Delta Ct}$ method. The obtained expression data were analyzed, using online services (http://www.sabiosciences.com/), the program mayday-2.14 [32], and the Genesis program [33].

3. Results and discussion

3.1. X-ray photoelectron spectroscopy (XPS)

XPS method is widely used for analysis of PEEK surfaces treated by different techniques (e.g. Refs. [5,34–37]). Plasma treatment of polymer has been shown to increase the surface oxygen content, particularly carbonyl/ester and carboxyl type groups. Relative ratio of different chemical groups containing oxygen at the PEEK surface was estimated in Refs. [5,16]. XPS analysis of the ANAB-treated PEEK surface revealed bond rearrangements on both the carbon (C_{1S}) as well as the oxygen (O_{1S}) spectra. Shifts were calculated with respect to the carbon binding energy in aromatic compounds of 284.7 eV (0.3 eV lower than in aliphatic ones).

In the control PEEK sample (Fig. 1A), the shifts were +7.97 eV and −1.1 eV. The binding energy of the main oxygen peak was 532.35, which corresponds to the aliphatic oxygen in the ether compounds. Qualitative composition of carbon: about 96% aromatic, about 4% bound to oxygen in aliphatic orientation. In the ANAB-treated PEEK sample (Fig. 1B), the shifts were +7.27 eV and −1.75 eV. The binding energy of the maximum peak of oxygen was 532.2–532.4 (for each of the pairs of peaks), which corresponds to the ether oxygen in both the aromatic and aliphatic compounds respectively. Qualitative composition of carbon: about 90% aromatic, about 10% bound in aliphatic orientation to oxygen.

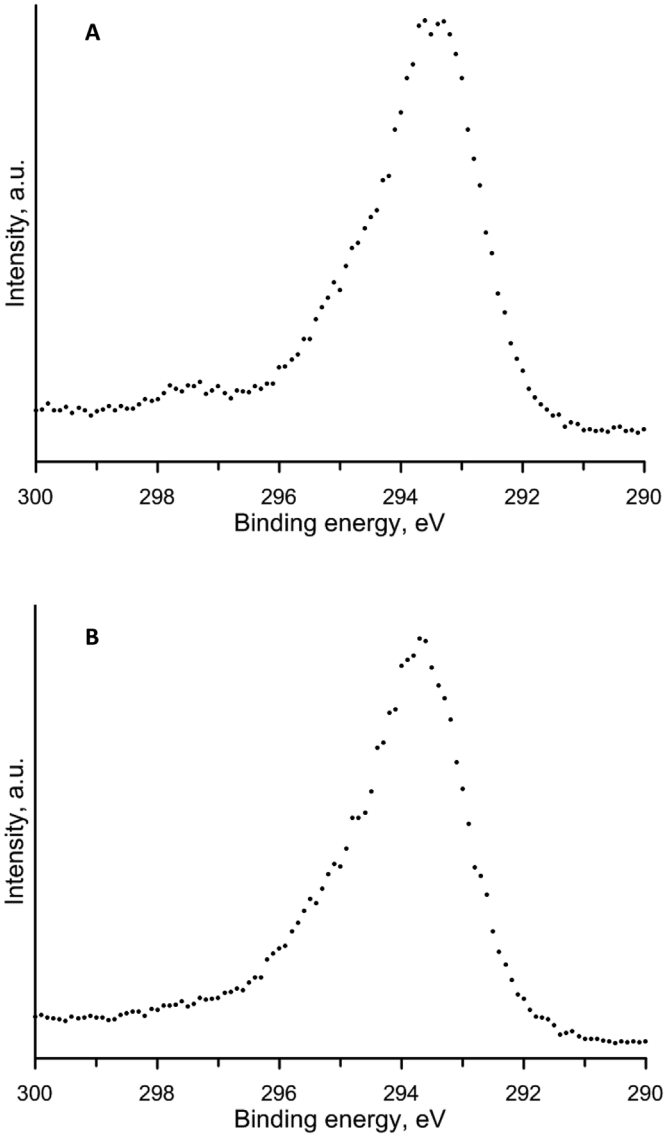

Fig. 1. XPS C1s spectra for control (A) and ANAB-modified (B) samples. Changes in binding energies suggest minor bond rearrangements including additional carboxyl ends.

In general, the spectra are similar, the peaks consist of the same components. Relative amounts of oxygen and various forms of carbon are reproduced well; there is no addition or modifications to the chemical composition, however, the binding energy of the oxygen spectra increases in a few fragments: CH_2—O—, C═O, C(arom)—O—. This may be similar to other techniques where an increase in carboxyl groups is observed, thereby potentially increasing cell attachment.

3.2. IR spectroscopy

Samples of control and ANAB-treated PEEK were investigated by IR Fourier spectroscopy. A method of specular reflection is well suited for studying the surface of this material since it is characterized by the

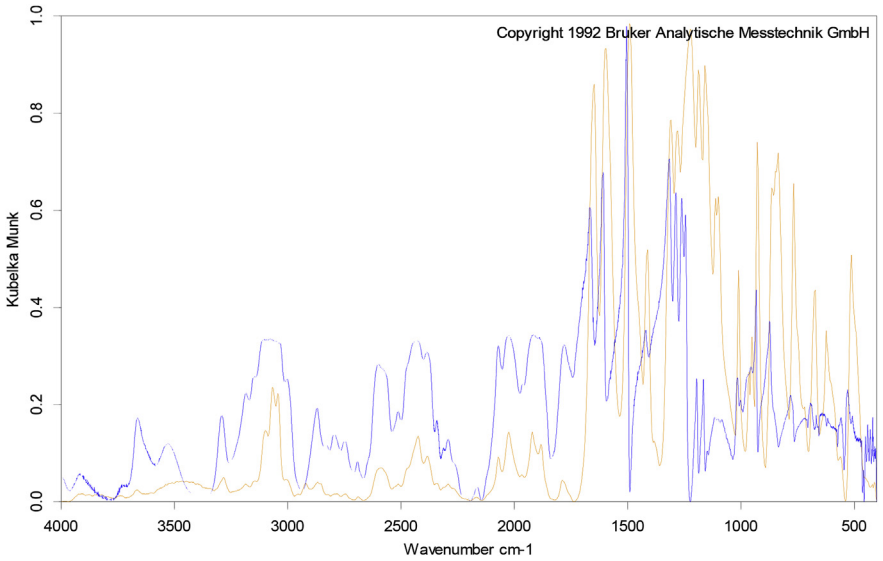

Fig. 2. IR Fourier spectrum of the library spectrum of PEEK (The Hummel Infrared Standards Distributed by Chemical Concepts, Weinheim, Germany COPYRIGHT (C) 1991 D.O.HUMMEL, ICP UNIVERSITY COLOGNE, GERMANY; orange line) as compared with the ANAB-treated PEEK sample (blue line).

lowest depth of penetration among all methods of recording IR spectra available to us. The spectra obtained by specular reflection are a superposition of the reflection and transmission spectra. Usually the best results are obtained with an angle of incidence of radiation of the order of 45° and with a coating thickness of about 0.01 mm. Fig. 2 shows the IR spectra of the ANAB-treated PEEK sample (blue) compared to the library spectrum for PEEK (orange). The presence of an aromatic group is found in the bands 3030 and 1600-1500 cm^{-1}, the nature of the substitution is determined by absorption below 900 cm^{-1}.

The presence of a group corresponding to ethers with aromatic substituents is confirmed by absorption in the region of 1280–1010 cm^{-1}. The carboxyl group is found by intensive absorption at 1664 cm^{-1}, which very well corresponds to the data for aromatic ketones. In addition, it should be noted that the sample contains free water, the presence of which is easily detected by absorption in the region of 3330–3700 cm^{-1}.

The spectrum of both the control and ANAB-treated PEEK sample are in good agreement with the library spectrum of the PEEK of the trademark Talpa-K-200, CAS No. 108568-51-0, studied in the form of a beige crystalline film. The absorption in the 2700-2200 cm^{-1} region refers to the crystallinity bands. Samples of the control and the ANAB treated PEEK have practically the same IR spectra in that region.

3.3. Surface wettability

The surface charge and its wettability determine the surface proteomic profile, and subsequently the interaction with cells through the adsorption of the adhesive proteins of the serum [38]. Contact angle measurements of wettability are essential evaluations of biomaterial properties [39]. Polymer surfaces with a high content of $-CH_3$, $-CH{=}CH_2$ groups form hydrophobic surfaces ($\theta_a > 80^o$), while $-COOH$, $-NH_2$-groups form moderately hydrophobic surfaces (θ_a = 48-62^o) and -PEG and $-OH$ groups form hydrophilic surfaces ($\theta_a < 35^o$). Attachment and cell spreading is most pronounced on moderately hydrophobic surfaces (θ_a = 48-62^o), while hydrophobic or nonionic hydrophilic surfaces inhibit interaction with cells.

Measurement of the stationary contact angle of wetting showed a significant change in the wettability of the surface of PEEK polymer films exposed to ANAB treatment as compared to the untreated surface. The average value (n = 10) of the contact angle of water surface wetting decreased from 92.4 ± 8.5° on the untreated surface to 72.9 ± 4.5° for the ANAB-treated PEEK surface. The contact angle of physiologic saline solution surface wetting decreased from 87.6 ± 2.4° on the untreated surface to 66.1 ± 4.3° for the ANAB-treated PEEK surface. The contact angle of FBS surface wetting decreased from 79.0 ± 9.1° on the untreated surface to 60.4 ± 5.8° for the ANAB-treated PEEK surface. There was no significant difference between the values of the contact angles of wetting the surface with different liquids. At the same time, all three series of measurements showed significant differences in the contact angles of the ANAB-treated and untreated PEEK surfaces (Fig. 3).

3.4. Surface morphology

The issue of regulating surface roughness is important for developing new biomaterials and optimizing substrate properties for the growth of mammalian cells. Even small changes in the substrate surface profile can lead to a change in the cellular response, ranging from an increase in cellular activity to a significant inhibition. It has been shown that the surface roughness at the nanometer level affects the adhesion and proliferation of cells on the substrate, determines the motor activity of cells and the degree of their polarization, and affects the synthesis of

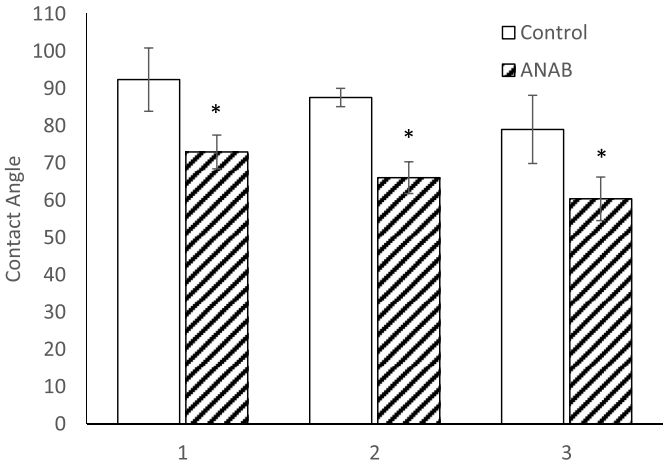

Fig. 3. Surface wettability of the control surface (white bars) and ANAB-treated PEEK surface (hatched bars) with different liquids: 1- deionized water; 2- physiologic saline solution; 3- fetal bovine serum. ANAB-treatment results in significantly (*, p < 0.02) more hydrophilic surface for all liquids tested.

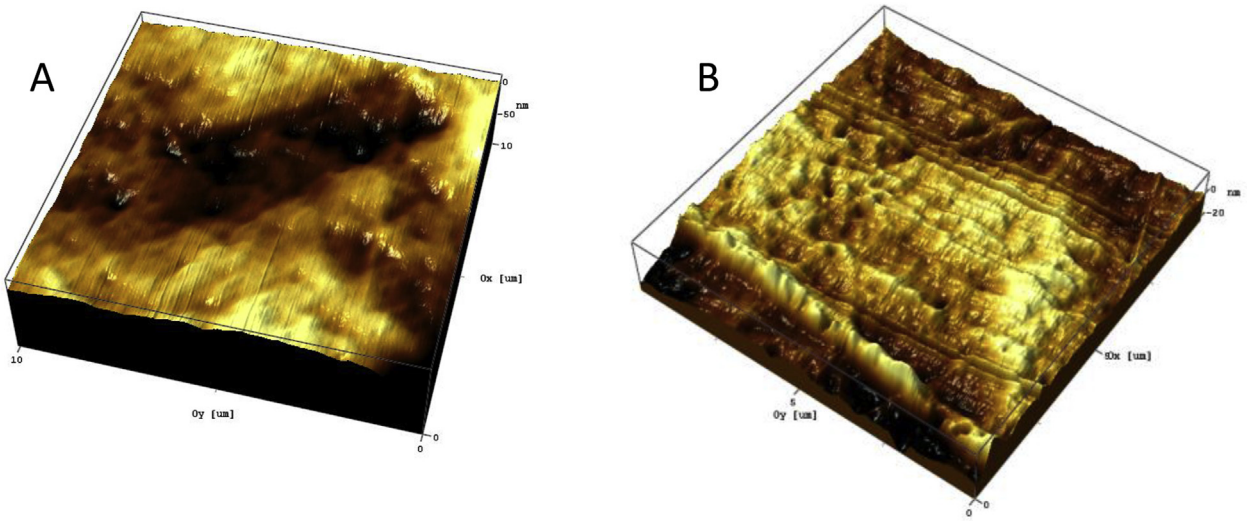

Fig. 4. AFM analysis of the surface profile of the initial (A) and ANAB modified (B) surface of the PEEK film, (10 μm resolution); (A) Ra = 4.63 ± 0.78 nm; (B) Ra = 3.45 ± 0.52 nm. Although ANAB-treated PEEK surface is smoother as seen by Ra, a nano-scale topography is apparent.

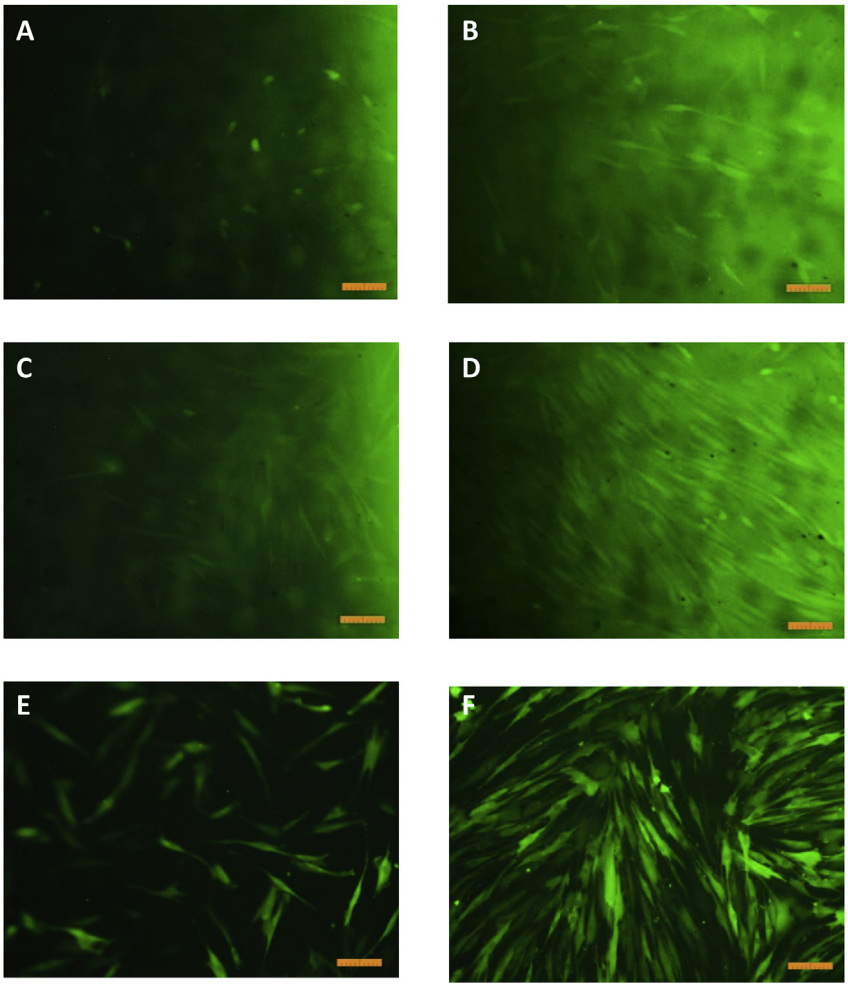

Fig. 5. The appearance of DPSC cells (ALU-GFP, by fluorescent microscope) growing on the untreated (A, B) and ANAB-treated (C, D) surfaces of PEEK, after 24 h (A, C) and after three days (B, D) after inoculation. Appearance of DPSC cells (ALU-GFP) cultivated on the surface of the cover glass after 24 h (E) and after three days (F) after inoculation. 100 μm bar.

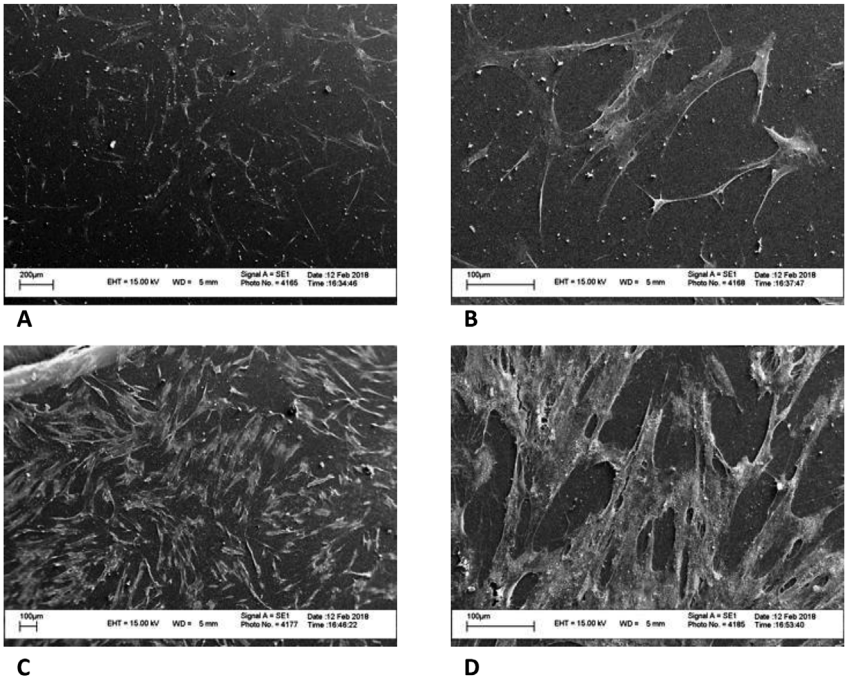

Fig. 6. Scanning electron microscopy (SEM) images of DPSC cells cultivated on the untreated (A, B) and ANAB-treated surfaces (C, D) of PEEK, 24 h after seeding.

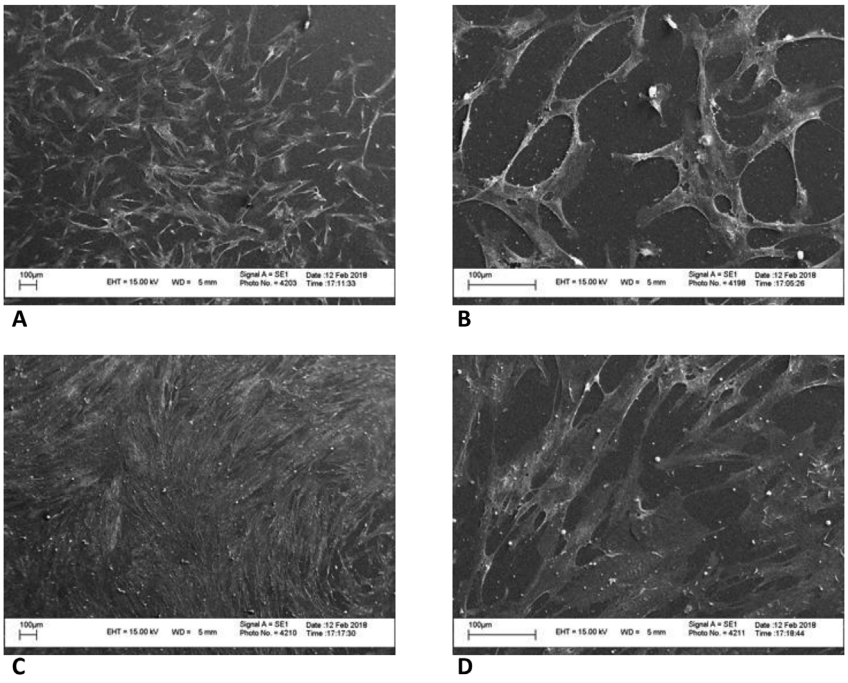

Fig. 7. SEM images of DPSC cells cultivated on the untreated (A, B) and ANAB-treated surfaces (C, D) of PEEK, 72 h after seeding.

specific proteins [40]. The influence of substrate nanotopography on cell gene expression and differentiation has been pointed out, but little is known about the interplay of these cues [41–43]. Mechanisms that regulate cell behavior and differentiation are poorly understood due to differences in cell type, substrate material, geometry and parameters measured.

In this study, we show a slight decrease in the average surface roughness of ANAB-treated PEEK (Fig. 4B, Ra = 3.45 ± 0.52 nm) as compared to the control sample (Fig. 4A, Ra = 4.63 ± 0.78 nm). However, the ANAB-treated PEEK displays a more textured surface profile, which may cause a significant change in the wettability of the surface as well as promoting the adhesion of proteins and cell proliferation.

3.5. Viability, adhesion and proliferative activity of human DPSC on the surface of PEEK

The viability and distribution of DPSCs on the treated and untreated surfaces were visualized using SYTO9 staining at days 1 and 3. We found that cells were well spread and randomly distributed onto the entire surface of the samples. The proliferation of cells was observed on both the control and ANAB-treated samples at 1 and 3 days after seeding and was confirmed by the results of DPSCs adhesion density. At day 3 there was significant difference in the viability and cell adhesion

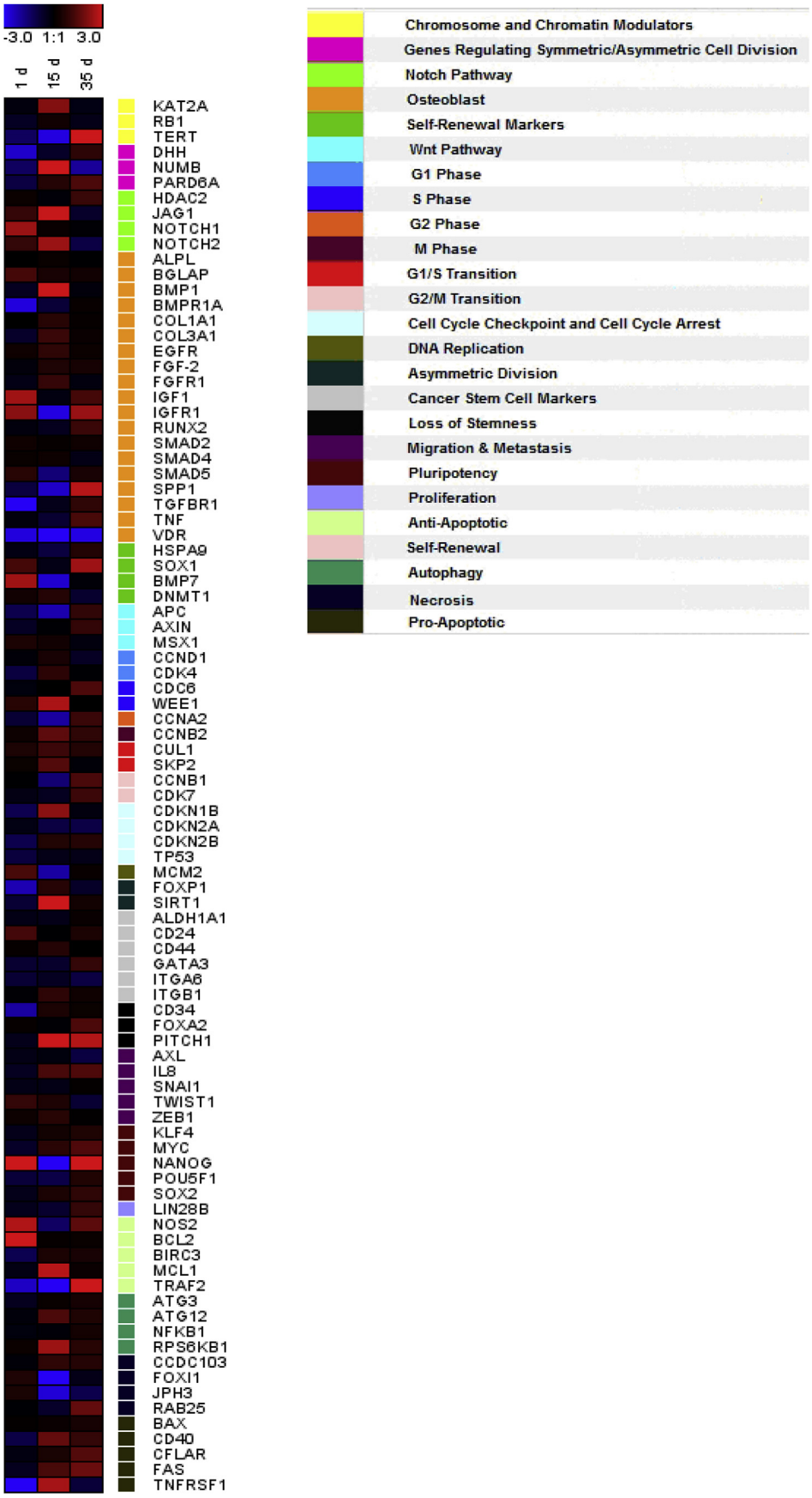

Fig. 8. Change in gene expression in cells growing on ANAB-treated surface in comparison with control PEEK at 1, 15 and 35 days after seeding. Color gradations from black to blue reflect the degree of inhibition of gene expression, gradation from black to red represent the level of upregulation with respect to controls. Genes are color grouped based on functionality.

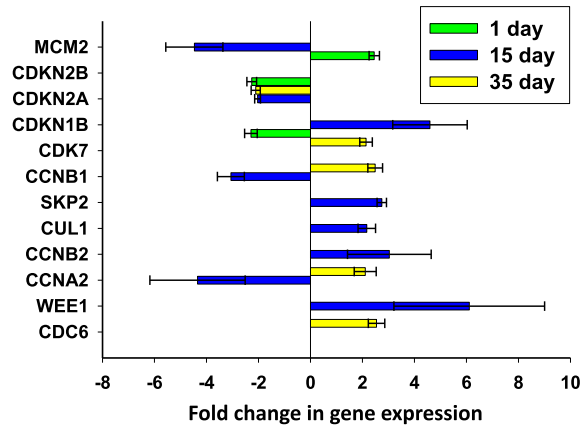

Fig. 9. Changes in the expression of proliferation markers of DPSC growing on ANAB-treated PEEK in relation to control PEEK. Many of the proliferation genes are upregulated in response to the ANAB surface.

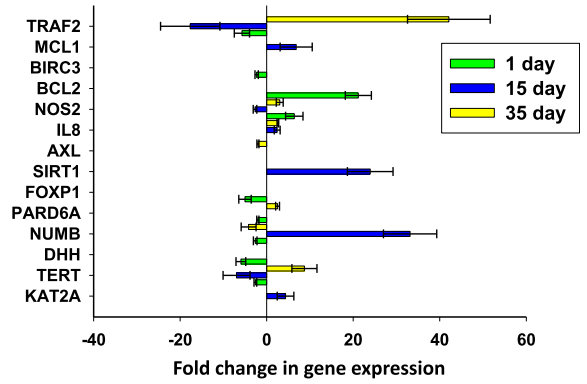

Fig. 10. Changes in the expression of anti-apoptosis, cells division and migration markers of DPSC growing on ANAB-treated PEEK in relation to control PEEK.

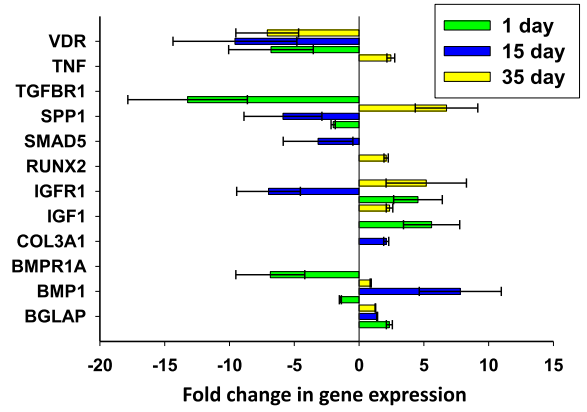

Fig. 11. Changes in the expression of differentiation markers of DPSC growing on ANAB-treated PEEK in relation to control PEEK. Many of the genes responsible for osteogenesis are upregulated in response to the ANAB surface.

between ANAB-treated and untreated surfaces, with significantly higher adhesion density and number of cells on the ANAB-treated surface compared to untreated surface (Figs. 5–7).

3.6. Gene expression study

The phenotypic expression profile of cells growing on the surface of control and ANAB-treated PEEK was evaluated by real-time PCR.

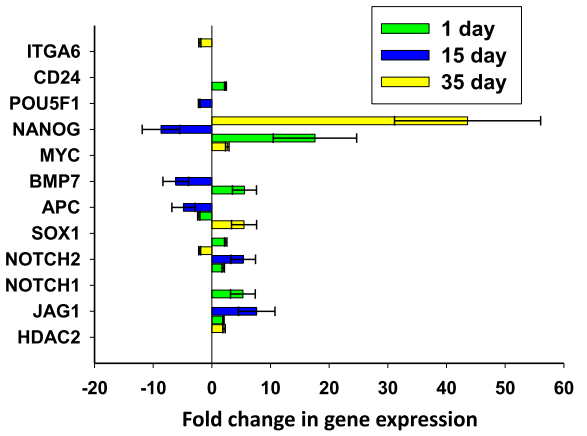

Fig. 12. Changes in the expression of self-renewal and stemness markers of DPSC growing on ANAB-treated PEEK in relation to control PEEK. Several genes involved in maintenance of stemness are upregulated in response to the ANAB surface.

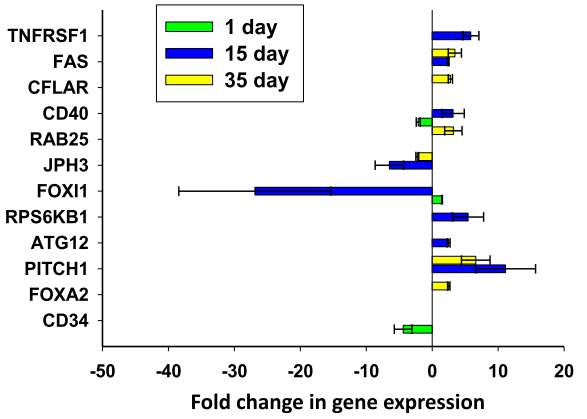

Fig. 13. Changes in the expression of stem reduction, autophagy, necrosis and pro-apoptosis markers of DPSC growing on ANAB-treated PEEK in relation to control PEEK.

Expression of marker genes reflecting the processes of proliferation and differentiation, maintenance of stem capacity, apoptosis and necrosis was investigated. The process of cell differentiation usually requires at least 2 weeks. We determined the starting level of gene expression of DPSCs on day 1 after seeding and investigated the level of change on days 15 and 35, which made it possible to identify the change dynamics of the expression of 92 human genes responsible for various intracellular processes on the surface of control and ANAB-treated PEEK. We found differences in the expression of several genes (Fig. 8). Gene affiliations to identify different clusters and markers are shown using a color scale (Fig. 8).

Expression of the house-keeping genes *ACTIN*, *RPLP* and *GAPDH* served as internal controls for all subsequent assays. Real-time quantitative PCR analysis of the expression levels of proliferation markers (Fig. 9) identifies that on day 15, CDKN1B, SKP2, CUL1, CCNB2 and WEE1 gene expression were significantly higher on ANAB-treated PEEK than on the untreated surface. On day 35, ANAB-treated surfaces result in upregulation of the CDC6, CCNA2, CCNB and CDK7 genes. These results are in agreement with the visual data collected (Figs. 5–7).

Expression levels of anti-apoptosis, division, and cell migration markers of DPSCs on ANAB-treated PEEK (Fig. 10) showed early stage decreased expression for regulators of the fission symmetry and chromatin modulators (TERT, DHH, NUMB). At the same time, expression of the anti-apoptosis genes NOS2 and BCL2 were upregulated. On day 15, the greatest transcriptional activity was observed for the genes NUMB,

SIRT1 (symmetry of cell division) and MCL1 (anti-apoptosis). It is also worth noting the very high level of expression of the anti-apoptotic marker TRAF2 observed on day 35 which was downregulated at the earlier time points. Increased levels of expression of the differentiation marker genes - TNF, TGFBR1, RUNX2, IGFR1, IGF1, BMP1 and BGLAP were observed on ANAB-treated PEEK (Fig. 11), showing that cells are differentiating towards osteoblasts. At the same time, VDR transcription activity decreased significantly, which indicates that the cells do not reach terminal differentiation.

Transcription of self-renewal markers and stemness on the ANAB processed surface for JAG1, NOTCH1, NOTCH2, SOX1, BMP7, NANOG and CD24 genes (Fig. 12) was upregulated at day 1. By day 15, the increased level of JAG1, NOTCH2 gene transcription was maintained on the ANAB-processed surface but was reduced for BMP7 and NANOG. However, NANOG, MYC, and SOX1 were once again upregulated at day 35. This indicates that some cells retain their stemness for a potentially longer time when growing on the ANAB-treated surface as compared to control. At day 15 and 35, we observed an increase in the transcriptional activity of the stem-reduction markers genes (FOXA3 and PITCH1, Fig. 13), and the expression of the pro-apoptosis markers (FAS, TNFRSF1 and CFLAR) and one marker of necrosis (RAB25) on ANAB-treated surfaces. Thus, judging by the transcription activity, the ANAB treatment of the surface stimulated the cells to osteogenic differentiation, while the cells retained a high status of stem and mitotic activity.

At an early stage of cell growth on the ANAB treated PEEK surface, compared with the untreated, a reduced level of transcription of the TERT, DHH, NUMB, PARD6A, BMPR1A, TGFBR1, VDR, APC, CDKN1B, CDKN2B, FOXP1, CD34, BIRC3, TRAF2, CD40 and TNFRSF1 genes was observed. The increased expression level was in NOTCH1 genes, BGLAP, IGF1 and IGFR1 and some others (SOX1, MCM2, CD24, NANOG, NOS2, BMP7, BCL2) markers of osteogenesis. With longer culture, the transcription activity of most genes did not differ with the growth of cells on the ANAB untreated and treated material, but for individual osteogenesis marker genes (BMP1, COL3A1, IGF1, IGFR1, RUNX2, SPP1, TNF), the growth of cells on the ANAB treated material resulted in an increase in transcriptional activity genes. Also, in the cells on the ANAB treated material, the concentration of the mRNA of TERT and NANOG (pluripotency markers) and TRAF2 (an anti-apoptosis marker) was significantly increased. It should be noted that in the cells on the processed PEEK, the transcriptional activity of proliferation markers increased (CDC6, WEE1, CCNA2, CCNB2, CUL1, SKP2, CCNB1, CDK7).

4. Conclusions

We have shown that exposure to ANAB treatment affects the biological activity of cells cultured under *in vitro* conditions on the PEEK surface. Change in the average roughness of the ANAB-treated PEEK surface in the absence of a change in the chemical composition of the surface, led to an increase in the wettability of the surface of the polymer film. We have shown that when human DPSC cells grow on a nanotextured ANAB modified surface, there is an increase in cellular adhesion and proliferative activity, and an increase in the level of protein expression and activity of the cytoskeleton. ANAB processing of the PEEK surface does not change the chemical structure of the material, but it does modify its hydrophilic-hydrophobic properties due to changes in the surface roughness. The moderate-hydrophilic surface of the polymer subjected to ANAB processing promotes the adhesion and growth of human dental pulp stem cells and their differentiation in the osteogenic direction.

The comparison of the expression pattern of marker genes that reflect the processes of proliferation and differentiation, maintenance of stem cells, apoptosis and necrosis, at different times of culture of DPSC cells on the surface of modified and unmodified PEEK showed that isolated cells are more sensitive even to nano-scale surface roughness.

Our studies show that regulating surface roughness is important for the development of new biomaterials, since even small changes in the surface profile of the implant can lead to a change in its hydrophilic-hydrophobic properties and cellular response. A new method for modifying the surface of polymeric materials using accelerated neutral atom beam technology can improve the biological activity of polymer materials for implantation without changing the chemical composition of the surface.

This ANAB surface modification can enhance PEEK biomaterials that have better physical attributes such as modulus of elasticity or radiolucency, however, are inert. ANAB-treated PEEK, therefore, could be used as a replacement material both untreated PEEK as well as titanium, for patients that have metal sensitivity. Future long-term studies in animal models will be pursued to evaluate *in vivo* effects.

Conflict of interest

Joseph Khoury, Ph.D.: 1) is employed by Exogenesis Corp; 2) holds stock in Exogenesis Corp.

Sean Kirkpatrick: 1) is employed by Exogenesis Corp; 2) holds stock in Exogenesis Corp.

Dmitry Shahkov, Ph.D.: 1) is employed by Exogenesis Corp; 2) holds stock in Exogenesis Corp.

No other authors have a conflict of interest.

Acknowledgments

The present work was partially performed with the financial support of the Ministry of Education and Science of the Russian Federation (RFMEFI57417X0136). We wish to thank Bontham Phok for ANAB treatment of PEEK materials and Richard Svrluga for guidance on the initiation of the project.

References

[1] S.M. Kurtz, J.N. Devine, PEEK biomaterials in trauma, orthopedic, and spinal implants, Biomaterials 28 (32) (2007) 4845–4869, https://doi.org/10.1016/j.biomaterials.2007.07.013.

[2] H.J. Münch, S.S. Jacobsen, J.T. Olesen, T. Menné, K. Søballe, J.D. Johansen, J.P. Thyssen, The association between metal allergy, total knee arthroplasty, and revision: study based on the Danish knee arthroplasty register, Acta Orthop. 86 (3) (2015) 378–383, https://doi.org/10.3109/17453674.2014.999614.

[3] D. Briem, S. Strametz, K. Schröder, N.M. Meenen, W. Lehmann, W. Linhart, A. Ohl, J.M. Rueger, Response of primary fibroblasts and osteoblasts to plasma treated polyetheretherketone (PEEK) surfaces, J. Mater. Sci. Mater. Med. 16 (7) (2005) 671–677, https://doi.org/10.1007/s10856-005-2539-z.

[4] S.W. Ha, M. Kirch, F. Birchler, K.L. Eckert, J. Mayer, E. Wintermantel, C. Sittig, I. Pfund-Klingenfuss, M. Textor, N.D. Spencer, M. Guecheva, H. Vonmont, Surface activation of polyetheretherketone (PEEK) and formation of calcium phosphate coatings by precipitation, J. Mater. Sci. Mater. Med. 8 (11) (1997) 683–690, https://doi.org/10.1023/A:1018535923173.

[5] A.E. Wiącek, K. Terpiłowski, M. Jurak, M. Worzakowska, Effect of low-temperature plasma on chitosan-coated PEEK polymer characteristics, Eur. Polym. J. 78 (2016) 1–13, https://doi.org/10.1016/j.eurpolymj.2016.02.024.

[6] K. Terpiłowski, A.E. Wiącek, M. Jurak, Influence of PEEK nitrogen plasma treatment for wettability of deposited chitosan layers, Adv. Polym. Technol. 37 (6) (2018) 1557–1569, https://doi.org/10.1002/adv.21813.

[7] Y. Zhao, H.M. Wong, W. Wang, P. Li, Z. Xu, E.Y. Chong, C.H. Yan, K.W. Yeung, P.K. Chu, Cytocompatibility, osseointegration, and bioactivity of three-dimensional porous and nanostructured network on polyetheretherketone, Biomaterials 34 (37) (2013) 9264–9277, https://doi.org/10.1016/j.biomaterials.2013.08.071.

[8] J.H. Lee, H.L. Jang, K.M. Lee, H.R. Baek, K. Jin, K.S. Hong, J.H. Noh, H.K. Lee, In vitro and in vivo evaluation of the bioactivity of hydroxyapatite-coated polyetheretherketone biocomposites created by cold spray technology, Acta Biomater. 9 (4) (2013) 6177–6187, https://doi.org/10.1016/j.actbio.2012.11.030.

[9] S.W. Ha, A. Gisep, J. Mayer, E. Wintermantel, H. Gruner, M. Wieland, Topographical characterization and microstructural interface analysis of vacuum-plasma-sprayed titanium and hydroxyapatite coatings on carbon fibre-reinforced poly(etheretherketone), J. Mater. Sci. Mater. Med. 8 (12) (1997) 891–896, https://doi.org/10.1023/A:1018562023599.

[10] B.D. Hahn, D.S. Park, J.J. Choi, Osteoconductive hydroxyapatite coated PEEK for spinal fusion surgery, Appl. Surf. Sci. 283 (2013) 6–11, https://doi.org/10.1016/j.apsusc.2013.05.073.

[11] A. Rabiei, S. Sandukas, Processing and evaluation of bioactive coatings on polymeric implants, J. Biomed. Mater. Res. A. 101 (9) (2013) 2621–2629, https://doi.org/10.1002/jbm.a.34557.

[12] M.S. Abu Bakar, M.H. Cheng, S.M. Tang, S.C. Yu, K. Liao, C.T. Tan, K.A. Khor, P. Cheang, Tensile properties, tension-tension fatigue and biological response of polyetheretherketone-hydroxyapatite composites for load-bearing orthopedic implants, Biomaterials 24 (13) (2003) 2245–2250, https://doi.org/10.1016/S0142-9612(03)00028-0.
[13] M.S. Abu Bakar, P. Cheang, K.A. Khor, Mechanical properties of injection molded hydroxyapatite-polyetheretherketone biocomposites, Compos. Sci. Technol. 63 (3–4) (2003) 421–425, https://doi.org/10.1016/S0266-3538(02)00230-0.
[14] P. Cheng, K.A. Khor, Addressing processing problems associated with plasma spraying of hydroxyapatite coatings, Biomaterials 17 (5) (1996) 537–544.
[15] T.P. Chaturvedi, An overview of the corrosion aspect of dental implants, Indian J. Dent. Res. 20 (2009) 91–98.
[16] J. Khoury, M. Maxwell, R.E. Cherian, J. Bachand, A.C. Kurz, M. Walsh, M. Assad, R.C. Svrluga, Enhanced bioactivity and osseointegration of PEEK with accelerated neutral atom beam technology, J. Biomed. Mater. Res. Part B 105 (2017) 534–543.
[17] S. Ajami, M.J. Coathup, J. Khoury, G.W. Blunn, Augmenting the bioactivity of polyetheretherketone using a novel accelerated neutral atom beam technique, J. Biomed. Mater. Res. Part B 105 (2017) 1438–1446.
[18] A. Kirkpatrick, S. Kirkpatrick, M. Walsh, S. Chau, M. Mack, S. Harrison, R. Svrluga, J. Khoury, Investigation of accelerated neutral atom beams created from gas cluster ion beams, Nucl. Instrum. Methods Phys. Res. B 307 (2013) 281–289, https://doi.org/10.1016/j.nimb.2012.11.084.
[19] I. Yamada, J. Khoury, Cluster ion beam processing: review of current and prospective applications, Mater. Res. Soc. Symp. Proc. 1354 (2011) 21–32, https://doi.org/10.1557/opl.2011.1081.
[20] C.D. Wagner, W.M. Riggs, L.E. Davis, J.F. Moulder, G.E. Muilenberg, Handbook of X-Ray Photoelectron Spectroscopy, Perkin-Elmer Corp., 1979.
[21] B.V. Crist, Handbook of Monochromatic XPS Spectra: the Elements and Their Native Oxides, Wiley-Blackwell, 2000.
[22] Data base CASA XPS (http://www.casaxps.com/).
[23] J.H. Scofield, Theoretical Photoionization Cross Sections from 1 to 1500 keV, Lawrence Livermore National Laboratory Rep. UCRL-51326, (1973).
[24] P.J. Cumpson, Thickogram: a method for easy film thickness measurement in XPS, Surf. Interface Anal. 29 (6) (2000) 403–406, https://doi.org/10.1002/1096-9918(200006)29:6<403.
[25] PC Program QUASES-IMFP-Tpp2m (S. Tougaard, Ver. 3.0), (April, 2016) http://www.quases.com/products/quases-imfp-tpp2m/.
[26] S. Tanuma, C.J. Powell, D.R. Penn, Calculations of electron inelastic mean free paths. V. Data for 14 organic compounds over the 50–2000 eV range, Surf. Interface Anal. 21 (3) (1994) 165–176, https://doi.org/10.1002/sia.740210302.
[27] OPUS_6.0 (www.bruker.com).
[28] E. Pretsch, P. Buehlmann, M. Badertscher, Structure Determination of Organic Compounds: Tables of Spectral Data, 4 ed., Springer, 2009.
[29] J. Workman Jr., The Handbook of Organic Compounds. 3 Vols. Set. NIR, IR, R and UV-Vis Spectra Featuring Polymers and Surfactants, Elsevier, 2000.
[30] R.A. Poltavtseva, S.V. Pavlovich, I.V. Klimantsev, N.V. Tyutyunnik, T.K. Grebennik, A.V. Nikolaeva, G.T. Sukhikh, Y.A. Nikonova, I.I. Selezneva, A.K. Yaroslavtseva, V.N. Stepanenko, R.S. Esipov, Mesenchymal stem cells from human dental pulp: isolation, characteristics, and potencies of targeted differentiation, Bull. Exp. Biol. Med. 158 (1) (2014) 164–169, https://doi.org/10.1007/s10517-014-2714-7.
[31] J. Moffat, D.A. Grueneberg, X. Yang, S.Y. Kim, A.M. Kloepfer, G. Hinkle, B. Piqani, T.M. Eisenhaure, B. Luo, J.K. Grenier, A.E. Carpenter, S.Y. Foo, S.A. Stewart, B.R. Stockwell, N. Hacohen, W.C. Hahn, E.S. Lander, D.M. Sabatini, D.E. Root, A lentiviral RNAi library for human and mouse genes applied to an arrayed viral high-content screen, Cell 124 (6) (2006) 1283–1298.
[32] Program mayday-2.14. Center for Bioinformatics Tubingen, Germany.
[33] A. Sturn, J. Quackenbush, Z. Trajanoski, Genesis: cluster analysis of microarray data, Bioinformatics 18 (1) (2002) 207–208, https://doi.org/10.1093/bioinformatics/18.1.207.
[34] C. Jama, O. Dessaux, P. Goudmand, L. Gengembre, J. Grimblot, Treatment of poly ether ehter ketone (PEEK) surfaces by remote plasma discharge. XPS investigation of the ageing of plasma-treated PEEK, Surf. Interface Anal. 18 (1992) 751–756.
[35] S. Ha, R. Hauert, K. Ernst, E. Wintermantel, Surface analysis of chemically-etched and plasma-treated polyetheretherketone (PEEK) for biomedical applications, Surf. Coating. Technol. 96 (1997) 293–299.
[36] W.S. Ramsey, W. Hertl, E.D. Nowlan, N.J. Binkowski, Surface treatments and cell attachment, In Vitro 20 (1984) 802–808.
[37] T. Nakamura, H. Nakamura, T. Noguchi, K. Imagawa, Photodegradation of PEEK sheets under tensile stress, Polym. Degrad. Stabil. 91 (4) (2006) 740–746, https://doi.org/10.1016/j.polymdegradstab.2005.06.003.
[38] M. Abdallah, S.D. Tran, G. Abughanam, M. Laurenti, D. Zuanazzi, M.A. Mezour, Y. Xiao, M. Cerruti, W.L. Siqueira, F. Tamimi, Biomaterial surface proteomic signature determines interaction with epithelial cells, Acta Biomater. 54 (2017) 150–163, https://doi.org/10.1016/j.actbio.2017.02.044.
[39] G. Agrawal, Y.S. Negi, S. Pradhan, M. Dash, S.K. Samal, M.C. Tanzi, S. Fare (Eds.), Wettability and Contact Angle of Polymeric Biomaterials. Characterization of Polymeric Biomaterials, Woodhead Publ., Cambridge, 2017, pp. 57–81.
[40] E. Martínez, E. Engel, J.A. Planell, J. Samitier, Effects of artificial micro- and nano-structured surfaces on cell behavior, Ann. Anat. - Anatomischer Anzeiger 191 (1) (2009) 126–135, https://doi.org/10.1016/j.aanat.2008.05.006.
[41] K. Kulangara, Y. Yang, J. Yang, K.W. Leong, Nanotopography as modulator of human mesenchymal stem cell function, Biomaterials 33 (20) (2012) 4998–5003, https://doi.org/10.1016/j.biomaterials.2012.03.053.
[42] P.M. Tsimbouri, K. Murawski, G. Hamilton, P. Herzyk, O.C. cRichard, R.O.C. Oreffo, N. Gadegaard, M.J. Dalby, A genomics approach in determining nanotopographical effects on MSC phenotype, Biomaterials 34 (9) (2013) 2177–2184, https://doi.org/10.1016/j.biomaterials.2012.12.019.
[43] Wang P. Yu, H. Thissen, P. Kingshott, Modulation of human multipotent and pluripotent stem cells using surface nanotopographies and surface-immobilised bioactive signals: a review, Acta Biomater. 45 (11) (2016) 31–59, https://doi.org/10.1016/j.actbio.2016.08.054.